Neuroinform (2013) 11:249–257
DOI 10.1007/s12021-013-9179-0

ORIGINAL ARTICLE

Computer Aided Alignment and Quantitative 4D Structural Plasticity Analysis of Neurons

Ping-Chang Lee · Hai-yan He · Chih-Yang Lin · Yu-Tai Ching · Hollis T. Cline

Published online: 14 February 2013

Abstract The rapid development of microscopic imaging techniques has greatly facilitated time-lapse imaging of neuronal morphology. However, analysis of structural dynamics in the vast amount of 4-Dimensional data generated by in vivo or ex vivo time-lapse imaging still relies heavily on manual comparison, which is not only laborious, but also introduces errors and discrepancies between individual researchers and greatly limits the research pace. Here we present a supervised 4D Structural Plasticity Analysis (4D SPA) computer method to align and match 3-Dimensional neuronal structures across different time points on a semi-automated basis. We demonstrate 2 applications of the method to analyze time-lapse data showing gross morphological changes in dendritic arbor morphology and to identify the distribution and types of branch dynamics seen in a series of time-lapse images. Analysis of the dynamic changes of neuronal structure can be done much faster and with greatly improved consistency and reliability with the 4D SPA supervised computer program. Users can format the neuronal reconstruction data to be used for this analysis. We provide file converters for Neurolucida and Imaris users. The program and user manual are publically accessible and operate through a graphical user interface on Windows and Mac OSX.

Keywords Weighted match · Semi-automatic method · Dynamic analysis · Structural plasticity · Neuron morphology · In vivo time-lapse imaging · Dendrite dynamics

Ping-Chang Lee and Hai-yan He contributed equally.

Electronic supplementary material The online version of this article (doi:10.1007/s12021-013-9179-0) contains supplementary material, which is available to authorized users.

Y.-T. Ching (✉)
Department of Computer Science,
Institute of Biomedical Engineering,
National Chiao Tung University, Hsin Chu, Taiwan
e-mail: ytc@cs.nctu.edu.tw

H.-y. He · H. T. Cline (✉)
The Scripps Research Institute, The Dorris Neuroscience Center,
La Jolla, CA, USA
e-mail: cline@scripps.edu

C.-Y. Lin
Department of Bioinformatics, Chung Hua University,
Hsin Chu, Taiwan

P.-C. Lee
Industrial Technology Research Institute,
Hsin Chu, Taiwan

Introduction

The structures of neuronal dendrites and axons proscribe the connectivity neurons make within circuits and are therefore critical determinants of circuit function and plasticity (Halavi et al. 2012). Axonal and dendritic arbor structures change dramatically over time under natural circumstances, for instance, during development, aging, as a result of circuit plasticity or disease, and under experimental conditions, such as sensory deprivation or enhanced activity. Technical advances in vivo neuronal labeling methods and in vivo microscopy techniques, such as confocal and multi-photon laser scanning (Helmchen and Denk 2005; Wilt et al. 2009), have greatly facilitated imaging and acquisition of time-lapse data of changes in neuronal structure over time. These data have demonstrated that dynamic changes in neuronal structure can occur over the time-course of minutes to days to months (Cline 1999; Chen et al. 2011). Although 3 dimensional reconstruction of neuronal structure can be accomplished with computer assistance, analysis of dynamic structural changes in time-lapse image data sets remains a great challenge because of the difficulty of comparing two complex 3D neuronal arbors required to identify structural differences between them (He and Cline 2011).

To analyze detailed changes of 3D neuronal structures over time is a difficult task, partly because cumulative changes in the locations of individual branches can occur as a result of modest 3D shifts in positions or orientations of lower order branches, or

because minor differences in the position of the animal during in vivo imaging may shift the orientation of the neuron in the image. Most 4D analysis of neuronal structural dynamics from time-lapse imaging data is done by manual comparison of 2D or 3D reconstructions. To analyze the changes between two 3D reconstructions of neurons manually takes an expert hours to align and match the two reconstructed 3D complete dendritic arbor structures. Manual identification of the numbers and distribution of dynamic branches, categorized as retracted, newly added, transient, and stable, over a set of multiple images (Haas et al. 2006; Bestman and Cline 2009) is laborious and greatly slows down research in the field (He and Cline 2011). A computer method that assists in comparing 3D neuronal structures would address the weaknesses of manual analysis.

Recent work reported that computer-assisted automatic analysis of neuronal structures from time-lapse images could be achieved in cultured neurons (Al-Kofahi et al. 2006). This advance was facilitated by the 2D structure of cultured neurons and their relatively simple neuronal morphology. In this paper, we present a supervised 4D neuronal Structural Plasticity Analysis (4D SPA) computer method that computes precise changes in the positions and lengths of all neuronal branches in the arbor between two images or time-points and presents the data as an image superimposed on the 3D reconstruction of the neuron. The method is based on the identification of stable branch points, or 'significant points' in a pair of images, which are used as reference points to facilitate the alignment of the dendritic structures. We then decompose the neuronal arbor into subsets of branches, or subtrees, with each branch defined as the process extending from a significant point to the branch tip. Similarities between two branches at sequential time-points were then calculated, generating a suggestion list of potentially matching branches, which was then evaluated by the analyst. This method takes advantage of both the computer algorithm and human expertise to significantly reduce the time to identify matching branches in the sequential images and increases the reliability of the analysis results.

Methods

Data Preparation

Neurons from the optic tectum of *Xenopus laevis* tadpoles were labeled by expression of GFP (green fluorescent protein) and time-lapse images were acquired with a two-photon laser-scanning microscope, at either 4 h or 24 h intervals. Reconstruction of the entire dendritic arbor of the neurons was done by the computer-aided filament tracing function in the 3D image analysis software Imaris (Bitplane, USA) and the full filament data set was exported and converted into a txt file for dynamic analysis using the 4D SPA method. An example of a 3D image of a GFP-labeled neuron and the reconstructed dendritic arbor is shown in online resource Video 1. In the input txt file, the branches are represented as data points defined by their 3D location (coordinates) and are organized block-wise. Each block starts with a line defining the branch index (P #) and the number of nodes in that branch (N #). The first point is the starting point of the branch, either the soma or the branching point, and the last point in the block is the tip. The first point in the first block of the file represents the soma position. The detailed description of the input data format can be found in the manual of the 4D SPA (available through supplemental online resources). To facilitate usage of the SPA program, we made converting tools for reconstructed filament files generated from two of the most commonly used reconstruction software programs (Imaris and Neurolucida), which are also available through supplemental online resources.

Computer-Aided Comparison Method

A flow diagram of the program is shown in Fig. 1. The traced neuron, denoted N, is presented as a three-dimensional tree rooted at the soma, s. The tree structure data are composed of a series of vertices. The vertices in N are categorized into 3 sets: tips, regular points and branch points. The tips are the unbranched ends of branches in N denoted t_i, $1 \le i \le n$, where n is the number of tips. The branch points are vertices that have out degree, i.e. the number of

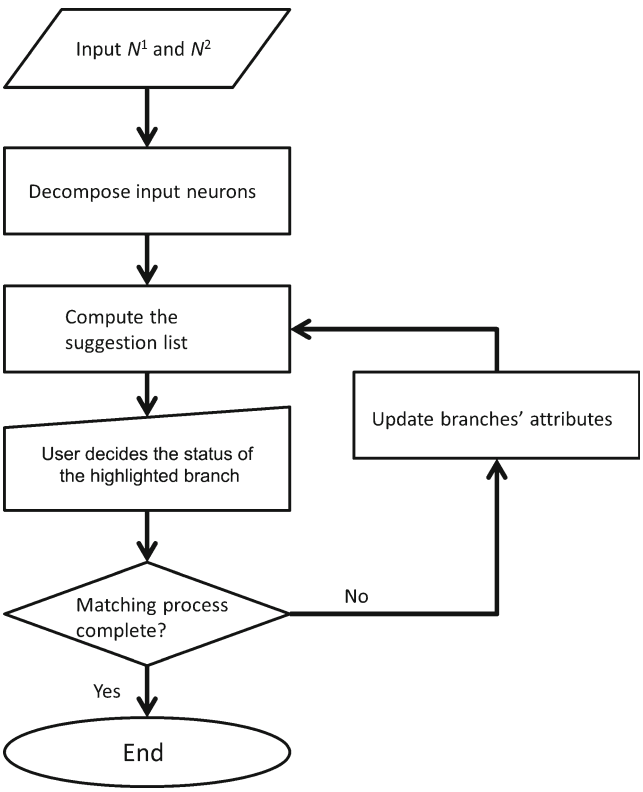

Fig. 1 Flow chart of the 4D SPA program

points directly connected to this point on the path away from the soma, greater than 1. All the other vertices are regular points in the neuronal structure. They have out degree equal to 1.

Branches are defined as following: For a pair of points u and v among all points in N, if there is a direct path $b=< u, p_1, p_2, \ldots, p_k, v >$, in which $p_1, p_2, \ldots, p_k$, are points in between u and v, the path length $L(b) = |\overline{u,p_1}| + \sum_{1 \le j < k} |\overline{p_j, p_{j+1}}| + |\overline{p_k, v}|$. We also use $<u,v>$ to denote the path b. If u is the soma or a branch point and v is a tip, then the path b is called a "branch" in N. To estimate the length of each branch, which will be used to compute the similarity between a pair of branches in two images, we resample points on the path between the branch point and the branch tip by arbitrarily counting the length between neighboring points as 1.

To facilitate comparison of the reconstructions of neuronal trees imaged at different time points, we need to define reference points or 'significant' points. Within the neuronal tree, each branch point can be considered as the root of a subtree (Fig. 2a). The size of a subtree is defined as the number of branch tips in that subtree. The "average tree size" of neuron N is then calculated by dividing the sum of the size of all subtrees within neuron N by the total number of branch points. A branch point, v, is defined as a "*significant*" point if 1. The size of any subtree, rooted at v is greater than the average tree size of the neuron; and 2. One of the following criteria is also satisfied:

1. There are more than 2 subtrees rooted at v.
2. There are only two subtrees rooted at v and the sizes of both subtrees are greater than 3.

Empirically, significant points, defined above, are usually stable over time and would exist in the dendritic trees of the same neuron at two consecutive time-points, thus can be used as reference points for alignment of the arbors (Fig. 2). In the following matching process, we first consider the branches emanating from a significant branch point b_i to a tip t_i where b_i is the closest significant point to t_i on the path from t_i to the soma. If there is no significant branch point along the path from t_i to the soma, then the soma is used as the starting point.

Branch Attributes

Each branch $b=< b_i, t_i>$has 3 attributes, the *length*, $L(b)$, the *parent*, and the *position*. The *parent* is either itself (the default value) or another branch $b'=< b_j, t_j>$that b attaches to. The *position* of b is deemed as undefined if the *parent* is itself. If the *parent* of b is b', then the *position* of branch b is defined as $L(< b_j, b_i >)/L(b')$. The *parent* and *position* of b are denoted as *parent* (b) and *position* (b) respectively. As mentioned earlier, the default *parent* of each branch is itself at the beginning of the matching process. During the matching process, the starting points of some branches change to the closest branch point or the soma if no other branch point is available along its path and their *parent*s are revised accordingly.

To compare a pair of branches between two images, the attributes, branch length, parent branch and position, are compared in a pre-screening step (the detailed pre-

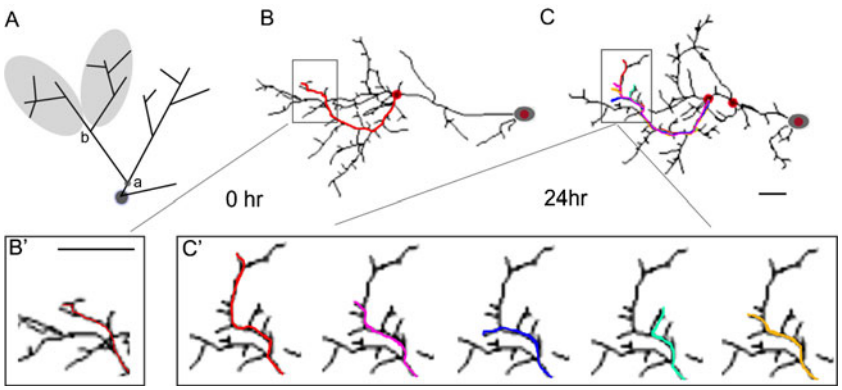

Fig. 2 Application of computer assisted 4D structural plasticity analysis to evaluate changes in dendritic arbor structure in neurons in daily time-lapse images. **a** Schematic drawing of the structure of a neuronal dendritic tree to illustrate the terminology used in this report. The soma is marked by the dark gray circle. Branch points are points where more than one branch is rooted, such as points a and b. All of the points along the branch path that are neither the branch point nor the branch tip are called regular points. There are altogether 13 branch points (including the soma) in the whole tree structure. The average tree size of the schematic neuron is 5.25, calculated as (3+4+2+3+4+8+2+2+3+5+13+14)/12; the tree sizes are listed in depth first traversal order. Branch point A is a 'significant point' because it has a subtree that is larger than the average tree size of the entire arbor and the size of both of its subtrees are larger than 3. Branch point B is not a 'significant point' since none of its subtrees (shaded in light gray) is larger than 5.25. **b**, **c** Reconstructions from a pair of images collected 24 h apart (data set No 5). The soma position is marked with the grey oval. Significant points are marked with filled red circles. To illustrate the branch matching process between arbors of 2 consecutive time-points, we colored one branch in the arbor from the first time-point in B in red (an amplified image of the dendritic part in the box is shown in B′). The five candidate matching branches provided by the algorithm in the arbor from the second time-point in C are shown in different colors to distinguish them from each other. Amplification of the boxed part is shown in C′ with each individual candidate matching branch. Scale bar: 10 μm

screening step is depicted in the following section). The similarity of the branches is taken into consideration only if the pair of branches pass the pre-screening. The similarity between two shapes is calculated by Eq. (1)

$$f(b_1, b_2) = \min_{R,\, v} \frac{1}{n} \sum_{x_i \in b_1, y_j \in b_2} \left\| Rx_i + v - y_j \right\|_2 + \max\left\{ \frac{L(b_1)}{L(b_2)}, \frac{L(b_2)}{L(b_1)} \right\} \quad (1)$$

where R is a rotation matrix and v is a translation vector. The number of points on b_1 is n. The value of $f(b_1, b_2)$ goes up when similarity goes down. The first term of Eq. (1) can be solved by the iterative closest pair method (Besl and MaKay 1992).

Pairwise Matching Analysis

For two reconstructions of the same neuron traced from image stacks acquired at different time-points, the first one is designated N^1 and the second one is designated N^2, in chronological order. During the matching process, branches in N^1 are categorized into 3 types, *remaining*, *retracted*, and *undefined*. A branch in N^1 is *remaining* if there is a matching branch in N^2. A branch is *retracted* if there is no matching branch in N^2. An *undefined* branch is a branch that has not been processed yet. Similarly, the branches in N^2 are also characterized into 3 types. The *remaining* and the *undefined* are the same as defined in N^1. There is no *retracted* branch category in N^2, instead, there are *newly added* branches, which refer to branches in N^2 that do not have a match in N^1.

Each iteration of the matching process consists of the following steps:

1. The longest undefined branch, B in N^1 is chosen.
2. For each undefined branch, $\widetilde{b} =< b_j, t_j >$ in N^2, we check its attributes. $\widetilde{b}$ is in the *candidate short list* if it satisfied all criteria listed below:
   a. Both B and $\widetilde{b}$ are *undefined* or *parent*(B) and *parent* ($\widetilde{b}$) are a matching pair;
   b. $\max\left\{ \frac{L(\widetilde{b})}{L(B)}, \frac{L(B)}{L(\widetilde{b})} \right\} < \alpha$;
   c. *position*(B)—*position*($\widetilde{b} < \beta$).
   α sets the upper limit of variation allowed in the branch length for the two branches being compared. β accounts for the largest variation allowed in the branch position on the parent branch. Both parameters help take into account the difference in structure caused by neuronal growth over the imaging time interval. The values are decided empirically and could be adjusted to optimize the program for specific applications. In all of our experiments we used the default setting set α=2.5 and β=0.4.

   The similarity (Eq. 1) between B and all branches in the *candidate short list* is calculated. The default setting of the length of the suggested list is limited to five, so at most, the most similar five branches will be included in the list. An example of the candidate branches in the suggestion list is shown in Fig. 1B, B′, C and C′.
3. The analyst then uses the suggestion list to assign a matching branch for B. If the analyst decides that B has a matching branch $\widetilde{b}$ in the candidate short list, B and $\widetilde{b}$ are moved into the remaining category. If the analyst decides that there is no matching branch for B, then B is assigned to the 'retracted' category. Based on the assignment of branches to categories, the attributes of some branches in both N^1 and N^2 are updated. The following is the update procedure for the branches in N^1 and N^2:
   a. If $L(B) < \gamma$, then the procedure stops. Here, γ stands for the minimum length (measuring from the closest branch point to the tip) a branch must have to be used for morphology comparison. This is because very short branches usually do not have many unique morphological features and could be easily confused with other non-matching short branches. The value of γ was determined empirically. During the course of our experiments, we set γ=15 μm.
   b. If $\widetilde{b}$ is categorized as *remaining* or *retracted*, no further process is needed.
   c. Assuming an *undefined* branch, $\widetilde{b} =< b_k, t_k >$ in N^1 has a common path with B and the conjunction point of B and $\widetilde{b}$ is $\widetilde{c}$, then $\widetilde{b}$'s *parent* and starting point become B and $\widetilde{c}$ respectively.
4. If there are no more *undefined* branches in N^1, then all of the remaining *undefined* branches in N^2 are changed to *newly added* and the process terminates. Otherwise, the iteration restarts from step 1.

A graphic-user interface (GUI) software system was implemented to help the analyst complete the matching process. Through the GUI, the analyst can decide the type of branch and set up parameters for the matching process.

Dynamics Branch Analysis

Pairwise analysis of sequential images in a longer time-lapse data set requires that branches have unique identifiers that are maintained through the image series. Initially, the branches are assigned an identifier or an "index" according to their *length* in descending order. After the analyst confirms all the matching branch pairs in N^1 and N^2, the 4D SPA program adjusts the indices so that matching branches

are assigned with the same identifier. To combine the multiple pairwise alignment results in data sets with more than 2 images, an extra step is added at the end of each comparison to synchronize the branch indices. This way, we can easily identify each individual branch in every time-point and analyze the dynamic changes of that particular branch over time.

Results

Ten data sets of fully reconstructed dendritic arbors were used in our experiments. The analyst was allowed to use two data sets to become familiar with the 4D SPA program. Then the time to analyze the remaining eight data sets was determined.

Pairwise Analysis

In this analysis, N^1 and N^2 are two reconstructed neuronal arbors imaged at consecutive time-points. Typically, for manual evaluation of structural dynamics in two images, the analyst identifies a branch in N^1, reviews all unmatched branches in N^2, and selects the best matching one. This process is extremely time-consuming and subjective. Our program generates a reliable short-list of suggested matching branch candidates in N^2 for every branch in N^1 based on the algorithm described above, which should greatly reduce the processing time. In addition, use of the same algorithm to generate the short list of suggested matching branch candidates helps to maintain consistent criteria to identify candidate matches and reduce human errors.

We quantified the reliability of the algorithm by calculating the *hit* ratio. For a branch in N^1, the 4D SPA method generates a list of suggested matching branches in N^2. We get a *hit* if one of the following two criteria is met.

1. The user decided there is no match, and the branch is identified as *retracted*, or
2. The user selected a matching branch from the suggested short list.

The hit ratio is calculated as the percentage of hits relative to the total number of branches in N^1, which measures the accuracy of the suggested match list. The analysis result for each data set is listed in Table 1. The mean number of branches on the suggested match list was 2.78 (Table 1). The average hit ratio was 85.8±8.4 % (Table 1). Note that dataset No5, which showed the highest hit ratio, is also the most complicated dataset with the largest total dendritic branch tip number. This indicates that the reliability of this matching program is not compromised by increased complexity of the neuronal structure. A pair-wise alignment result of representative dataset number 6 is shown in online resource Video 2. In this video, each frame displays both N^1 and N^2, and only one matching pair, which had been confirmed by the analyst, is rendered in red. Among all the data sets, data set number 9 had the lowest hit ratio (70.3 %) and the longest average list of the suggested matches. This is due to the high similarity between subtrees emanating from the same parent branch in N^1 and N^2 (Fig. 3). This combination (similarity in both subtree structure and the parent branch) tends to mislead the algorithm, thus might require more human intervention to locate the correct matching branch. The average time to align a pair of complete dendritic arbors was about 43 min (Table 1). In the worst case (dataset No5), it took 111 min to process a set of data. Given that this time includes both the time it takes by the program to do the calculation as well as the time it takes the analyst to validate the matches, it is understandable that the time increases with increased complexity of the dendritic arbor. Without the help of 4D SPA, it usually takes hours for an expert analyst to process a paired data set, depending on the complexity of the arbor and the magnitude of change between the two neuronal structures (He and Cline 2011).

Table 1 Parameters for 4D SPA data analysis results. Each data set contains a pair of neuronal dendritic arbors (reconstructed from the same neuron imaged at different time point, N1 and N2). Hit ratio measures the percentage of correct matches in the suggested list relative to the total branch number. Time records the total time taken for the analysis of that data set. Size of N1 (or N2) shows the total branch number of the dendritic arbor. Avg list size shows the average number of branches in the 'suggestion list' for each branch in N1 during the analysis of that data set. The first two data sets were used for the analyst to become familiar with the program, and thus were not included in the final calculations of the mean hit ratio, mean time, and mean Avg. list size, which are listed at the bottom of the table

Data	Hit ratio	Time (min.)	Size of N1	Size of N2	Avg. list size
1	0.969	–	31	24	1.407
2	0.856	–	69	80	2.814
3	0.921	42	76	63	2.422
4	0.859	43	63	79	2.422
5	0.967	111	89	84	2.422
6	0.795	13	38	58	3.051
7	0.917	46	58	59	3.483
8	0.758	44	60	80	3.515
9	0.704	35	80	94	3.741
10	0.833	5	13	18	2.5

mean Hit ratio: 0.858±0.084

mean Time: 42.375 min

mean Avg. list size: 2.78

Dynamic Branch Analysis

This method can be easily applied to analyze data sets consisting of multiple time-points in which N^1 is aligned

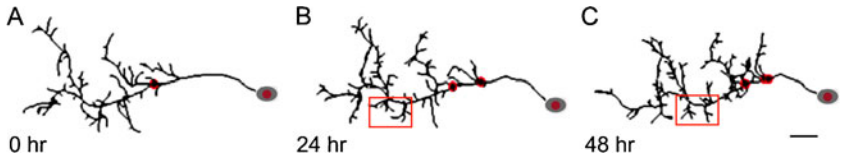

Fig. 3 Examples of subtree structure that is potentially confusing to the algorithm. A-C. Reconstructions of dataset numbers 8 and 9. Images were collected every 24 h over 3 days. The subtree structures that caused confusion to the program were marked with red boxes. The morphologies of these subtrees are very similar and they join the same parent branch right next to each other. This results in very similar attribute values for the branches and could increase the possibility of mismatching in the candidate list provided by the algorithm. This in turn might require more human intervention to identify the matching branch. Significant points are marked with filled red circles, and the soma is marked by dark grey circles. Scale bar: 10 μm

with N^2, then N^2 is aligned with N^3, …, and so on. Analysis of data sets with more than 2 time-points provides detailed analysis of branch dynamics, and often reveals important information about the underlying mechanisms of structural plasticity that are lost when long-interval data points are compared (Haas et al. 2006; Bestman and Cline 2008; Chiu et al. 2008). In the analysis of branch dynamics, branches are categorized as stable, newly added, retracted or transient. A stable branch is a branch that is present at all time-points. A retracted branch is a branch that is present at the first time-point but is lost at a later time-point. A 'newly added' branch is a branch that does not exist at the first time-point but appears later and remains in place until the last time-point. The 'added' branch category includes those that appear at the last time point. A transient branch is a branch that appears at a time-point after the first time-point and is then retracted by the last time-point. To better visualize the alignment results and branch dynamics, we implemented a color-coding system for the final display of the matching results. The *stable* branches are coded black, the *retracted* branches are blue, the *transient* branches are magenta, and the *newly added* branches are green (Fig. 4). This implementation facilitates the identification of qualitative changes in branch dynamics as well as possible spatial patterns of dynamic changes in the dendritic arbor over time. The results of the dynamic analysis can be exported as a spreadsheet for further analysis (Table 2). In addition, the matched neuronal filament data can be saved as txt files with the categorization information for each branch and used for further analysis.

Discussion

We present a method to provide computer assisted 4D structural plasticity analysis (4D SPA) of neuronal dendritic arbors. Here, we describe a simple but efficient algorithm that takes advantage of the presence of relatively stable branch points within the neuronal arbor structure combined with their geometry to facilitate the analysis of dynamic changes in the neuronal structure. To precisely identify similar structures within the tree structure by computer algorithms is a very difficult problem, given the subtle difference the arbors could have at different time points, and artifactual differences caused by shifts in the position of the animal during imaging and other factors. To achieve

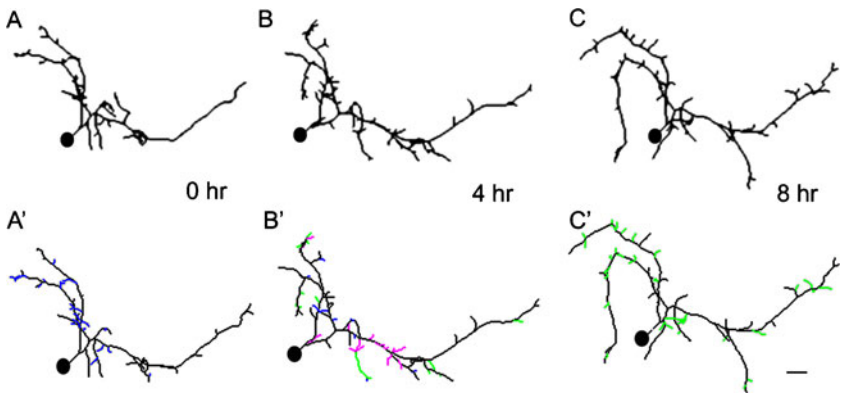

Fig. 4 Application of computer assisted 4D structural plasticity analysis to identify branch dynamics over relatively short time periods. A-C. Reconstructions of time-lapse imaging data of a representative optic tectal neuron imaged at 4 hour intervals. A′-C′. Computer generated reconstructions of the neuron at the timepoints corresponding to A-C to show the accuracy of the reconstruction generated by the 4D SPA program. Dendritic branches are color-coded according to their dynamic properties. The *stable* branches are black, the *retracted* branches are blue, the *transient* branches are magenta, and the *newly added* branches are green. Position of the neuronal soma is marked with the black oval. Scale bar: 10 μm

Table 2 An example of the output data spreadsheet of 4D SPA dynamic analysis results. Each branch is identified by an index number and categorized by its presence at a different time points of the time-lapse series (Type). The base length depicts the length from the soma to the branch tip at T0 (or from the soma to the last branch point in cases of newly-added and transient branches, which do not exist at T0). Change in the branch length, as measured from the last branch point to each branch tip at T1 and T2, are also listed

Index	Type	Base	T0	T1	T2
0	Retracted	108.347	0	−10.0098	−8.626
1	Retracted	100.107	0	−2.8265	[b]
2	Stable	96.2109	0	1.6266	0.856
3	Retracted	93.4048	0	0.1274	−3.0637
4	Stable	88.892	0	−1.2518	−10.9032
5	Stable	86.5705	0	−7.6944	13.0401
6	Stable	82.7616	0	−0.3493	−4.2367
7	Retracted	82.5884	0	−1.2502	[b]
8	Retracted	82.3081	0	−0.7123	−2.9365
9	Retracted	82.1164	0	−2.5229	[b]
10	Stable	78.0166	0	−19.886	−0.8122
11	Retracted	76.6955	0	−7.4872	−5.186
12	Retracted	69.4699	0	−4.4555	[b]
13	Stable	69.3531	0	0.8682	0.1089
14	Retracted	67.5669	0	−4.4827	[b]
15	Retracted	66.0081	0	−2.1148	[b]
16	Retracted	65.2153	0	−8.5441	[b]
17	Stable	64.1979	0	−8.8023	−0.4913
18	Retracted	63.9182	0	−11.6571	[b]
19	Retracted	63.2111	0	9.3652	−2.7323
20	Retracted	61.1388	0	−1.4803	[b]
21	Stable	59.4221	0	−2.7697	0.768
22	Stable	59.2012	0	10.917	7.5843
23	Stable	57.0635	0	−0.0772	−2.5156
24	Stable	54.485	0	1.5444	3.1327
25	Retracted	54.3478	0	−7.9197	[b]
26	Retracted	53.8825	0	−15.5446	[b]
27	Retracted	53.1091	0	−0.848	[b]
28	Retracted	52.8387	0	−8.7012	[b]
29	Stable	51.9241	0	1.8833	−5.6866
30	Retracted	49.4744	0	−1.5338	[b]
31	Stable	47.4518	0	0.2116	−1.0798
32	Stable	47.1564	0	−3.6643	1.3552
33	Retracted	40.5623	0	−6.8592	[b]
34	Retracted	36.5024	0	−9.9099	[b]
35	Stable	35.9169	0	0.1452	−1.761
36	Retracted	35.6123	0	−3.5941	[b]
37	Retracted	35.2614	0	−6.7228	[b]
38	Stable	35.0497	0	22.5963	−3.7935
39	Retracted	34.7067	0	−3.1454	[b]
40	Retracted	33.6457	0	1.4	−5.9116
41	Retracted	31.2966	0	−4.7041	[b]
42	Retracted	30.8287	0	−12.1339	[b]
43	Retracted	30.4663	0	−2.026	[b]
44	Newly-Added	75.7073	[a]	4.0313	−2.0182
45	Newly-Added	56.5727	[a]	4.7453	−5.4807
46	Transient	55.471	[a]	3.5334	−3.5334
47	Transient	55.471	[a]	3.0259	−3.0259
48	Transient	52.1022	[a]	5.5507	−5.5507

[a] branch not existing at T0

[b] branch already retracted at T1, thus not counted at T2

the most reliable result in an expeditious manner, we combined the advantages of the computer algorithm and the expertise of the human analyst. Instead of having the computer generate the final analysis, we use the computer algorithm to effectively narrow down the candidate list of the matching branches and let the human expert select the optimal match.

Many methods based on weighted-matching (Donte et al. 2004) and their applications to biomedical data have been reported (Dumay et al. 1992; Haris et al. 1999). We compared the performance of two automatic weighted-matching methods, the Hungarian algorithm and the greedy method, to our method, using the same data sets (data sets 3–10 in Table 1). The traced neuronal arbors were decomposed into sets of branches and Eq. (1) was used as the weighted function.

The processing time and the accuracy are two of the most important parameters to consider when comparing the matching methods. The average time cost per data set using the Hungarian algorithm was 90.4 min, which is more than twice the average processing time with our method. In addition, the accuracy of the Hungarian algorithm was far from perfect, which means that human verification and correction would be required. Online resource video 3 (Hugarian-ICP.avi) shows the matching result of data set No 6 reported by the Hungarian algorithm. The other automatic algorithm, the greedy method, was much faster. The average processing time was less than a minute. However, the accuracy of the matching results was poor. A representative video clip of the greedy method is shown in online resource video 4 (Greedy_ICP.avi). These results suggest that our strategy of combining the computer program with human supervision is indeed a highly efficient method.

4D SPA significantly increases the rate at which structural dynamics can be quantified and mapped onto the neuronal structure, and effectively reduces errors in the analysis and discrepancies between experimenters. As described in the methods section, there are three parameters (α,β,γ) used in the program that can be adjusted by the analyst to optimize

the algorithm to particular applications and cell types. For instance, higher values of α and β can be used if the images are taken over a longer time interval and the neuron is expected to have grown or changed a lot by the second time point. On the other hand, for relatively stable neuronal structures, smaller values would be preferred to reduce false positives on the list of suggested matching candidates. The value of γ can also be adjusted to better fit specific types of neurons with unique morphological features. The accuracy of the suggestion list decreases when the morphology of the subtrees connected to the same parent branch are highly similar, for instance in highly symmetric neuronal structures. In this case, extra care needs to be taken using the suggestion list. In cases where the real matching branch is not included in the suggestion list, we have implemented a manual assignment function in the program, which allows the analyst to pick any branch in N^2 and assign it as the matching branch for the branch in question.

4D SPA could easily be applied to neuronal axon arbors, which exhibit structural changes under a variety of conditions (Reh and Constantine-Paton 1985; Antonini and Stryker 1993; Cantallops et al. 2000; Cohen-Cory 2002; Ruthazer et al. 2003; De Paola et al. 2006). Other neuronal structures, such as the neuromuscular junction (Turney and Lichtman 2008), of which the morphological changes under different experimental conditions have been studied intensively, could also benefit from this tool. In addition, 4D SPA could be applied to study the structural dynamics of other cell types, the vasculature (Zhang et al. 2005) and extracellular space (Hochman 2012). In vivo time-lapse images of Xenopus radial glial cells collected at relatively short intervals have demonstrated rapid structural rearrangements of filopodia that were modulated by visual activity, NMDA receptor activity and nitric oxide signaling (Tremblay et al. 2009). Furthermore, images of Xenopus radial glial cells undergo significant structural changes during proliferation and neuronal differentiation (Bestman et al. 2012). In addition, immune cells are highly dynamic and their structural dynamics are essential to their function. In vivo imaging studies of microglia in rodent visual cortex demonstrate that they exhibit dynamic morphological rearrangements in response to visual deprivation and light exposure, suggesting an active role of microglial cells in experience-dependent synaptic modifications (Tremblay et al. 2010). Acute neuroinflamation in response to viral protein induces mobility of both leukocytes and microglia in the CNS, resulting in engulfment of synaptic structures and immune cells (Lu et al. 2011). As a final example, the CNS vasculature shows significant structural changes under healthy and diseased conditions (Carmeliet 2003; Zhang et al. 2005; Thal et al. 2012). Similar to efforts to automate reconstruction of neuronal structures, recent work has succeeded in automating reconstruction of vasculature from single time points (Zudaire et al. 2011), suggesting that comparisons of vasculature between timepoints could benefit from the algorithm presented here. Quantitative analysis of structural dynamics has been key to gaining insight into the mechanisms and function of dynamics in neurons. We anticipate that application of this algorithm to a variety of biological systems will be valuable.

Information Sharing Agreement

The software and user manual described in this work will be publicly accessible online at http://people.cs.nctu.edu.tw/~percycat/4DSPA/

Acknowledgments This work was funded by support from the National Institutes of Health (EY011261), the Hahn Family Foundation and the Nancy Lurie Marks Family Foundation to HTC, and the National Science Council, Taiwan, Grants 98-2221-E-009-118-MY3 and 101-2221-E-009-143-MY3 to Y-TC. We thank Dr. Shu-Ling Chiu for fostering this productive collaboration. P-CL would like to thank Dr. M. Giugliano for his help implementing the file converter.

Conflicts of Interest The authors declare that they have no conflict of interest.

References

Al-Kofahi, O., Radke, R. J., et al. (2006). Automated semantic analysis of changes in image sequences of neurons in culture. *IEEE Transactions on Biomedical Engineering, 53*(6), 1109–1123.

Antonini, A., & Stryker, M. P. (1993). Rapid remodeling of axonal arbors in the visual cortex. *Science, 260*(5115), 1819–1821.

Besl, P. J., & MaKay, N. D. (1992). A Method for Registration of 3-D Shapes. *IEEE Transactions PAMI, 14*(2), 239–256.

Bestman, J. E., & Cline, H. T. (2008). The RNA binding protein CPEB regulates dendrite morphogenesis and neuronal circuit assembly in vivo. *Proceedings of the National Academy of Sciences of the United States of America, 105*(51), 20494–20499.

Bestman, J. E., & Cline, H. T. (2009). The relationship between dendritic branch dynamics and CPEB-labeled RNP granules captured in vivo. *Front Neural Circuits, 3*, 10.

Bestman, J. E., Lee-Osbourne, J., et al. (2012). In vivo time-lapse imaging of cell proliferation and differentiation in the optic tectum of Xenopus laevis tadpoles. *The Journal of Comparative Neurology, 520*(2), 401–433.

Cantallops, I., Haas, K., et al. (2000). Postsynaptic CPG15 promotes synaptic maturation and presynaptic axon arbor elaboration in vivo. *Nature Neuroscience, 3*(10), 1004–1011.

Carmeliet, P. (2003). Angiogenesis in health and disease. *Nature Medicine, 9*(6), 653–660.

Chen, J. L., Lin, W. C., et al. (2011). Structural basis for the role of inhibition in facilitating adult brain plasticity. *Nature Neuroscience, 14*(5), 587–594.

Chiu, S. L., Chen, C. M., et al. (2008). Insulin receptor signaling regulates synapse number, dendritic plasticity, and circuit function in vivo. *Neuron, 58*(5), 708–719.

Cline, H. T. (1999). *Dendrite development in dendrites*. London: Oxford Univ. Press.

Cohen-Cory, S. (2002). The developing synapse: construction and modulation of synaptic structures and circuits. *Science, 298*(5594), 770–776.

De Paola, V., Holtmaat, A., et al. (2006). Cell type-specific structural plasticity of axonal branches and boutons in the adult neocortex. *Neuron, 49*(6), 861–875.

Donte, D., Foggia, P., et al. (2004). Thirty years of graph matching in pattern recognition. *IJPRAI, 18*, 265–298.

Dumay, A. C. M., R. J. Geest, et al. (1992). "Consistent inexact graph matching applied to labeling coronary segments in arteriograms." Proc.Int. Conf. Pattern Recognition Conf.: 439–442.

Haas, K., Li, J., et al. (2006). AMPA receptors regulate experience-dependent dendritic arbor growth in vivo. *Proceedings of the National Academy of Sciences of the United States of America, 103*(32), 12127–12131.

Halavi, M., Hamilton, K. A., et al. (2012). Digital reconstructions of neuronal morphology: three decades of research trends. *Frontiers in Neuroscience, 6*, 49.

Haris, K., Efstratiadis, S. N., et al. (1999). Model-based morphological segmentation and labeling of coronary angiograms. *IEEE Transactions on Medical Imaging, 18*(10), 1003–1015.

He, H. Y., & Cline, H. T. (2011). Diadem X: automated 4 dimensional analysis of morphological data. *Neuroinformatics, 9*(2–3), 107–112.

Helmchen, F., & Denk, W. (2005). Deep tissue two-photon microscopy. *Nature Methods, 2*(12), 932–940.

Hochman, D. W. (2012). The extracellular space and epileptic activity in the adult brain: explaining the antiepileptic effects of furosemide and bumetanide. *Epilepsia, 53*(Suppl 1), 18–25.

Lu, S. M., Tremblay, M. E., et al. (2011). HIV-1 Tat-induced microgliosis and synaptic damage via interactions between peripheral and central myeloid cells. *PloS One, 6*(9), e23915.

Reh, T. A., & Constantine-Paton, M. (1985). Eye-specific segregation requires neural activity in three-eyed Rana pipiens. *Journal of Neuroscience, 5*(5), 1132–1143.

Ruthazer, E. S., Akerman, C. J., et al. (2003). Control of axon branch dynamics by correlated activity in vivo. *Science, 301*(5629), 66–70.

Thal, D. R., L. T. Grinberg, et al. (2012). "Vascular dementia: Different forms of vessel disorders contribute to the development of dementia in the elderly brain." Experimental Gerontology.

Tremblay, M., Fugere, V., et al. (2009). Regulation of radial glial motility by visual experience. *Journal of Neuroscience, 29*(45), 14066–14076.

Tremblay, M. E., Lowery, R. L., et al. (2010). Microglial interactions with synapses are modulated by visual experience. *PLoS Biology, 8*(11), e1000527.

Turney, S. G., & Lichtman, J. W. (2008). Chapter 11: imaging fluorescent mice in vivo using confocal microscopy. *Methods in Cell Biology, 89*, 309–327.

Wilt, B. A., Burns, L. D., et al. (2009). Advances in light microscopy for neuroscience. *Annual Review of Neuroscience, 32*, 435–506.

Zhang, S., Boyd, J., et al. (2005). Rapid reversible changes in dendritic spine structure in vivo gated by the degree of ischemia. *Journal of Neuroscience, 25*(22), 5333–5338.

Zudaire, E., Gambardella, L., et al. (2011). A computational tool for quantitative analysis of vascular networks. *PloS One, 6*(11), e27385.